Electronic Supplementary Material (ESI) for Sustainable Energy & Fuels.

Binary Ni_2FeO_x anchored on modified graphite towards efficient and durable oxygen evolution electrocatalysis

Lu Bai, Jingqi Guan*

Experimental

Materials and reagents

All chemicals were analytical grade and used as purchased without further purification. Solutions were prepared using high purity water (Millipore Milli-Q purification system, resistivity > 18 MΩ•cm).

Synthesis of G-Ph

Typically, the dark gray graphite powder (0.5 g, 41.6 mmol of carbon) was dispersed in benzene (400 mL) in a 500 mL three necked round-bottom flask equipped with a magnetic stir bar. The contents were then stirred vigorously after benzoyl peroxide (10.1 g, 41.6 mmol) was added. The mixture was then heated at 80 °C for 12 h with continuous vigorous stirring. After cooling down, the contents of the flask were centrifuged and washed with ethanol for four times. The black solid was dried at 60 °C overnight, which was nominated as G-Ph.

Synthesis of G-Ph-SO_3H

The typical experimental processes include as follows: the phenylated graphite (G-Ph) (200 mg) was dispersed in oleum (70 mL, H_2SO_4, 25% as free SO_3), and heated at 80 °C for 5 h to yield phenyl sulfonated graphite. After cooling down, 300 g of ice block was then carefully added into the suspension. The mixture was then centrifuged and washed with water several times until the pH value of the filtrate reached ~7. The obtained solid was dried at 60 °C overnight, which was nominated as G-Ph-SO_3H.

Synthesis of Ni_nFeO_x@G-Ph-SN

Typically, stoichiometric $Ni(NO_3)_2$•$6H_2O$, 0.03 g $Fe(NO_3)_3$•$9H_2O$, 0.1 g G-Ph-SO_3H, and 50 μL of deionized water were added in 20.0 mL of ethanol solution. Under stirring, 75 μL of 28% ammonia was added to the mixture. Afterwards, it was transferred into 30 mL Teflon autoclave and heated at 150 °C for 2 h. After cooling down, the solid was obtained by filtering, washing with water for several times, and drying at 70 °C overnight, which was denoted as Ni_nFeO_x@G-Ph-SN (where n presents the atomic ratio of Ni/Fe). The loading content of Fe is ca. 4.0 wt.% measured by ICP-AES. The Ni content in $NiFeO_x$@G-Ph-SN, Ni_2FeO_x@G-Ph-SN, and Ni_3FeO_x@G-Ph-SN, is 3.9 wt.%, 7.7 wt.%, and 11.5 wt.% determined by ICP-AES.

Characterizations of samples

The as-prepared samples were characterized by X-ray powder diffraction (XRD) on a Rigaku D/Max-2500/PC powder diffractometer. The sample powder was scanned using Cu-Kα radiation with an operating voltage of 40 kV and current of 200 mA. The scan rate of 5°/min was applied to record the patterns in the range of 10-80°. Transmission electron microscope (TEM) images were observed by a Hitachi HT7700. High resolution TEM (HRTEM) images were recorded on a JEM-2100 transmission electron microscope (Tokyo, Japan) at 200 kV. The loading amount of manganese oxide in the catalyst was determined using inductively coupled plasma atomic emission spectrometer (ICP-AES) on a Shimadzu ICPS-8100. Prior to ICP-AES measurement, supported manganese oxide was dissolved in aqua regia. The valence state of cobalt oxide cluster was determined using XPS recorded on a Thermo ESCALAB 250Xi. The X-ray source selected was monochromatized Al Kα source (15 kV, 10.8 mA). Region scans were collected using a 20 eV pass energy. Peak positions were calibrated relative to C 1s peak position at 284.6 eV.

Electrochemical characterization

The electrochemical water oxidation performances of all the manganese-based electrodes were tested in a conventional three-electrode electrochemical cell with a platinum plate as the auxiliary electrode and a saturated calomel electrode (SCE, saturated KCl) as the reference electrode. 1 M KOH aqueous solution was used as

electrolyte with pH measured at ca. 13.6. The scanning rate was 5 mV/s. All potentials measured were calibrated to RHE using the following equation: E(RHE) = E(SCE) + 0.241V + 0.0591pH. The steady-state activity and long-term activity were evaluated by chronopotentiometry measurements. The ECSA was determined by measuring the capacitive current associated with doublelayer charging from the scan rate CV-dependence. Here, the CV potential window was 0.15 to 0.25 vs SCE. The scan rates were 20, 40, 60, 80, and 100 mV s^{-1}. The double-layer capacitance (C_{dl}) was estimated $\Delta j = (j_{charge} - j_{off\ charge})$ at 0.2 V vs SCE against the scan rate. The liner slop is twice of the double-layer capacitance C_{dl}. Electrochemical impedance spectroscopy (EIS) measurements were performed at open-circuit potential in the frequency range from 100 kHz to 0.1 Hz with an a.c. perturbation of 10 mV.

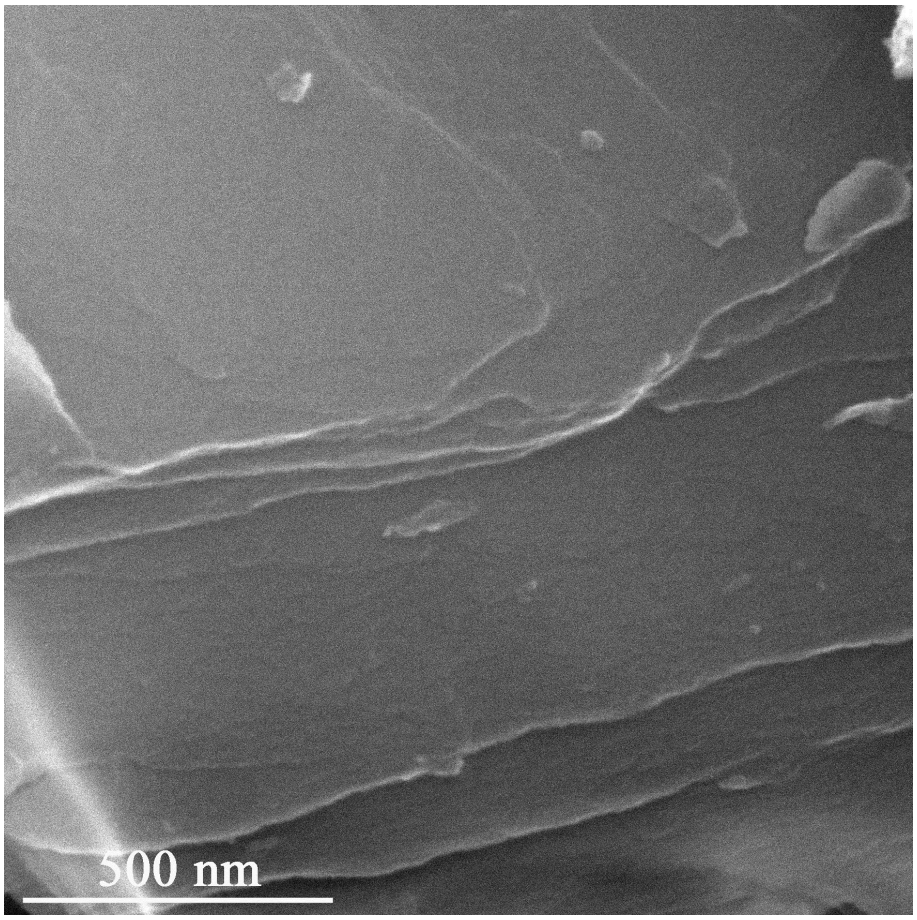

Figure S1. SEM image of G-Ph-SO_3H.

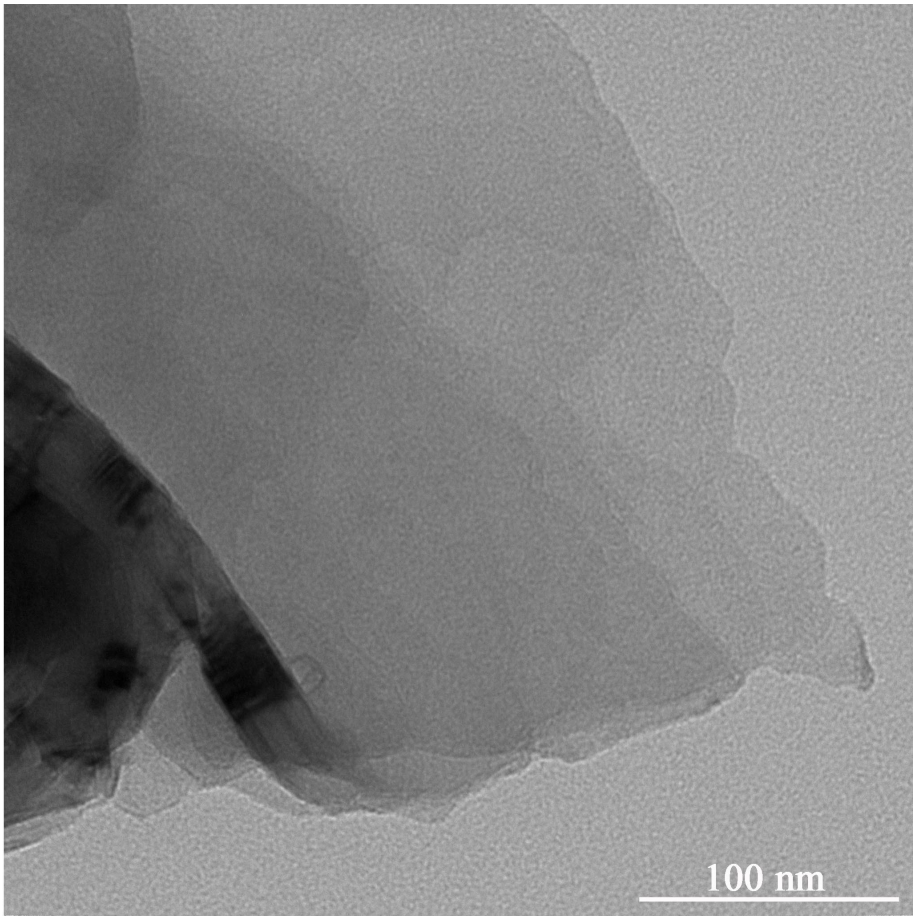

Figure S2. TEM image of G-Ph-SO_3H.

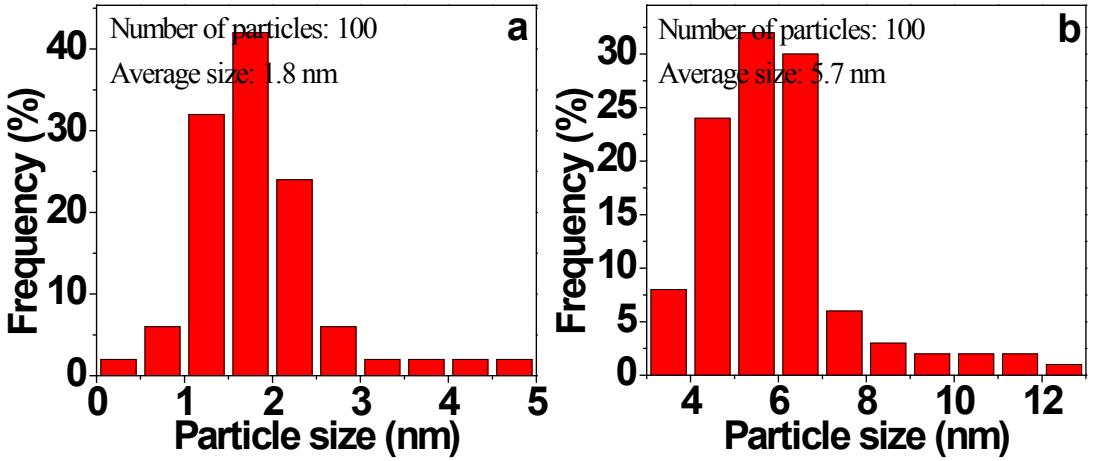

Figure S3. The histogram of size distribution of typical samples: FeO_x@G-Ph-SN (a), and NiO_x@G-Ph-SN.

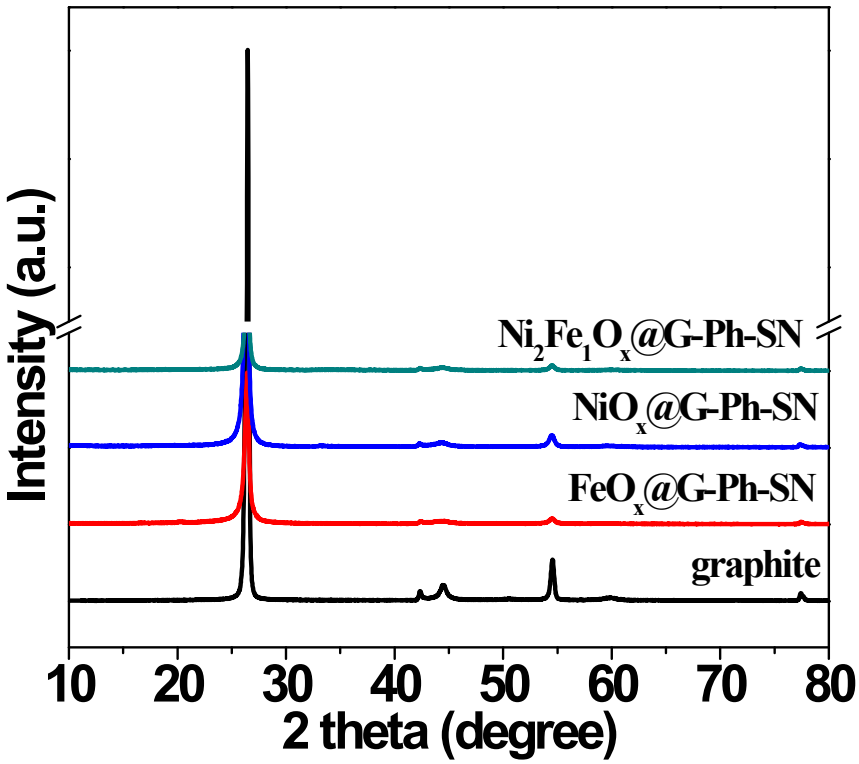

Figure S4. XRD patterns of graphite, FeO_x@G-Ph-SN, NiO_x@G-Ph-SN, and Ni_2FeO_x@G-Ph-SN.

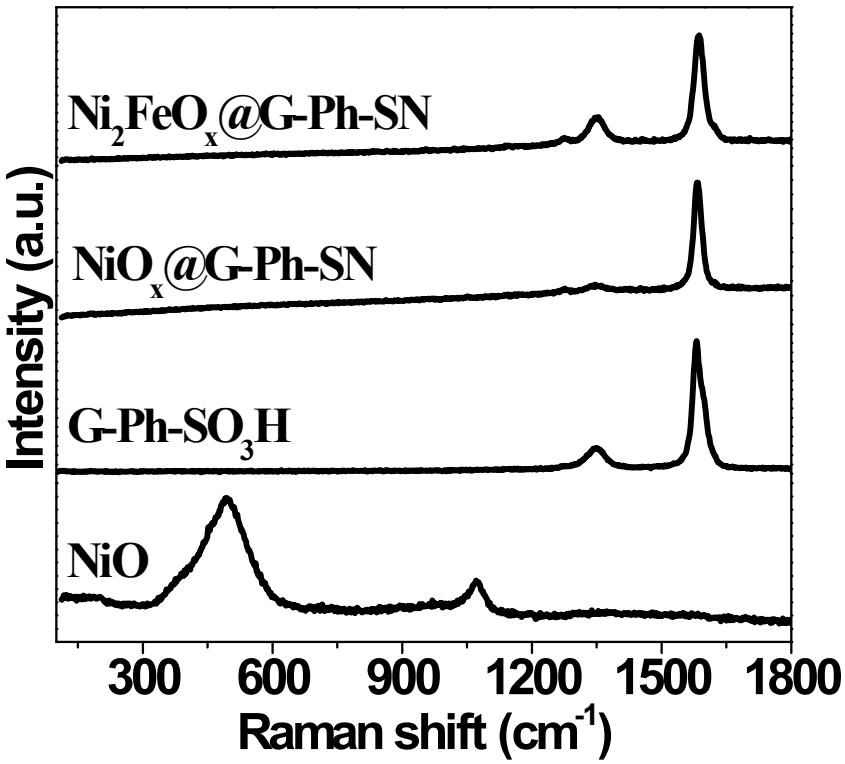

Figure S5. Raman spectra of NiO, G-Ph-SO_3H, NiO_x@G-Ph-SN, and Ni_2FeO_x@G-Ph-SN

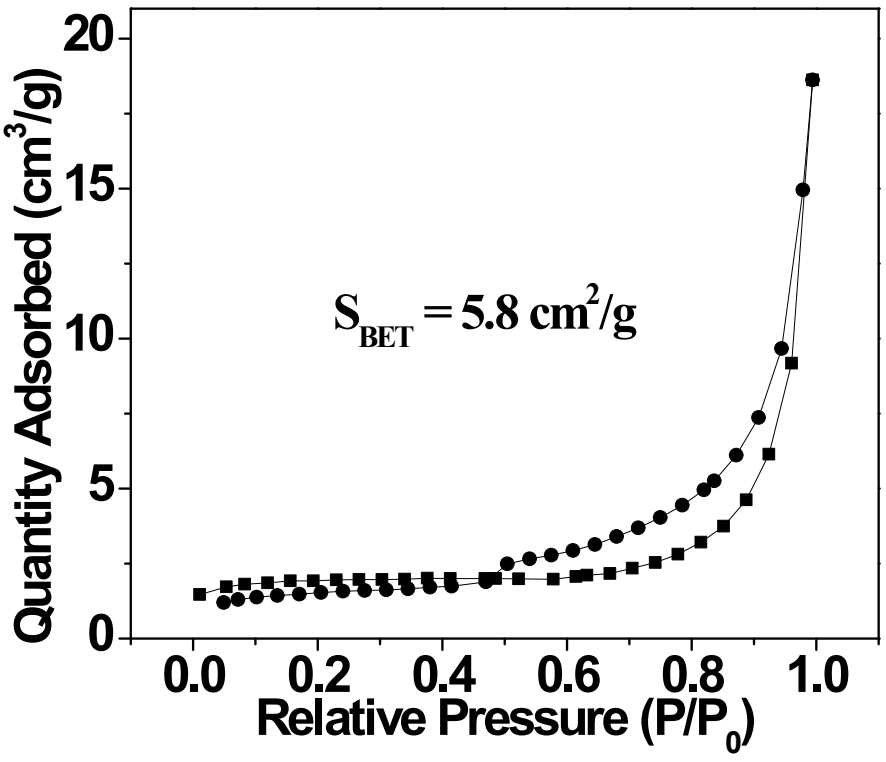

Figure S6. N_2 adsorption and desorption isotherms of the Ni_2FeO_x@G-Ph-SN sample.

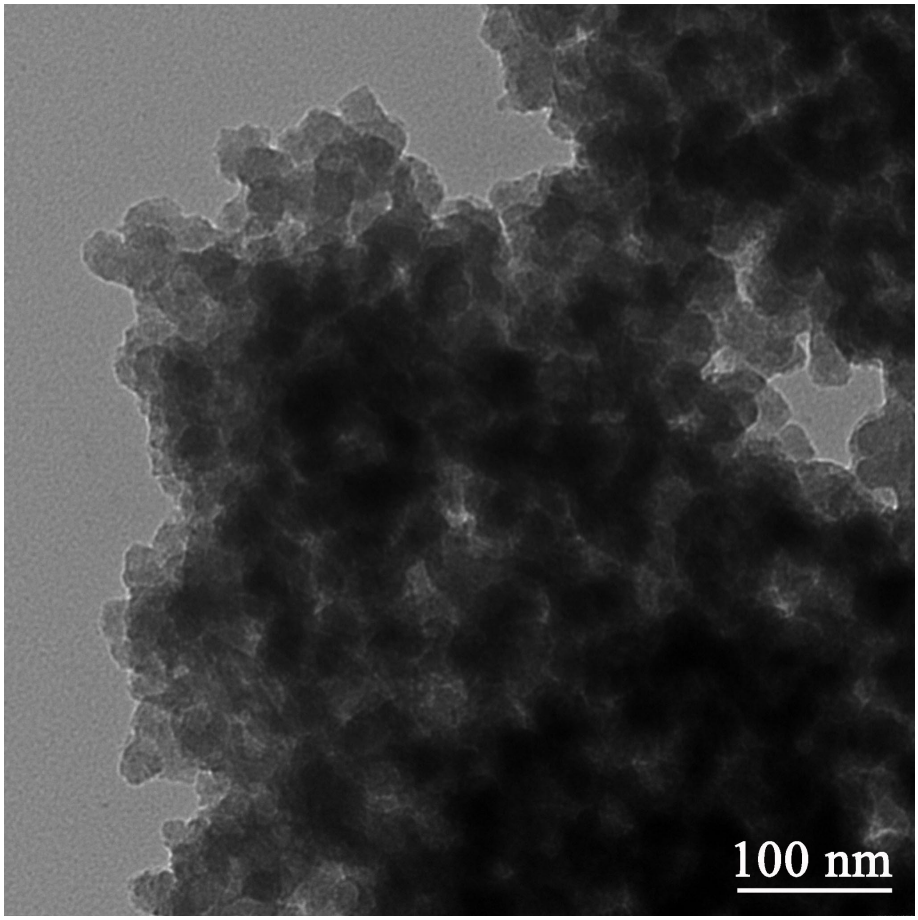

Figure S7. TEM image of IrO_2 nanoparticles.

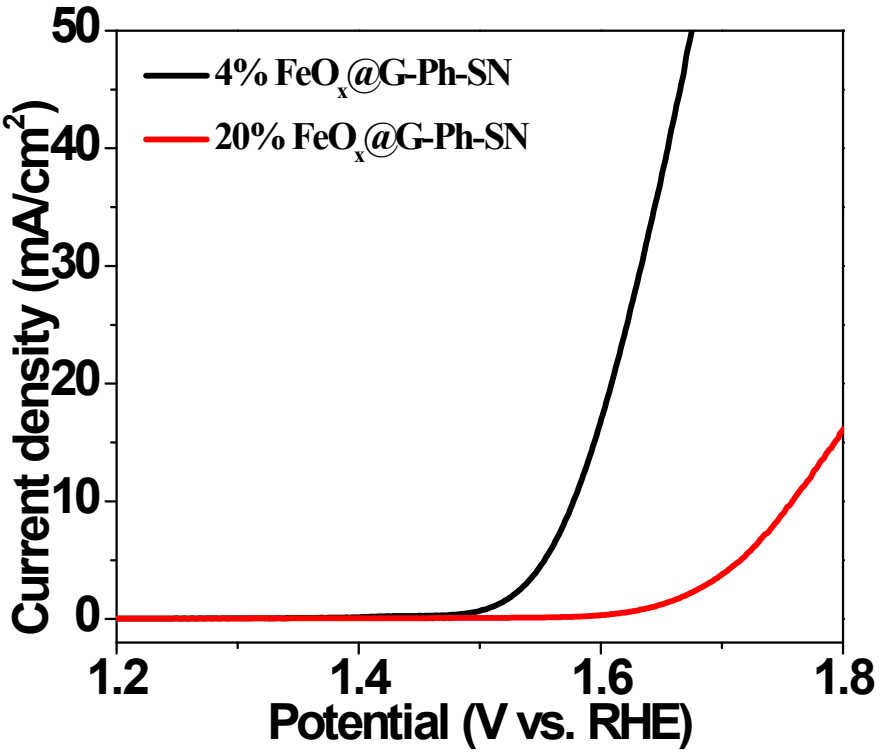

Figure S8. Polarization curves of FeO_x@G-Ph-SN with different Fe loadings.

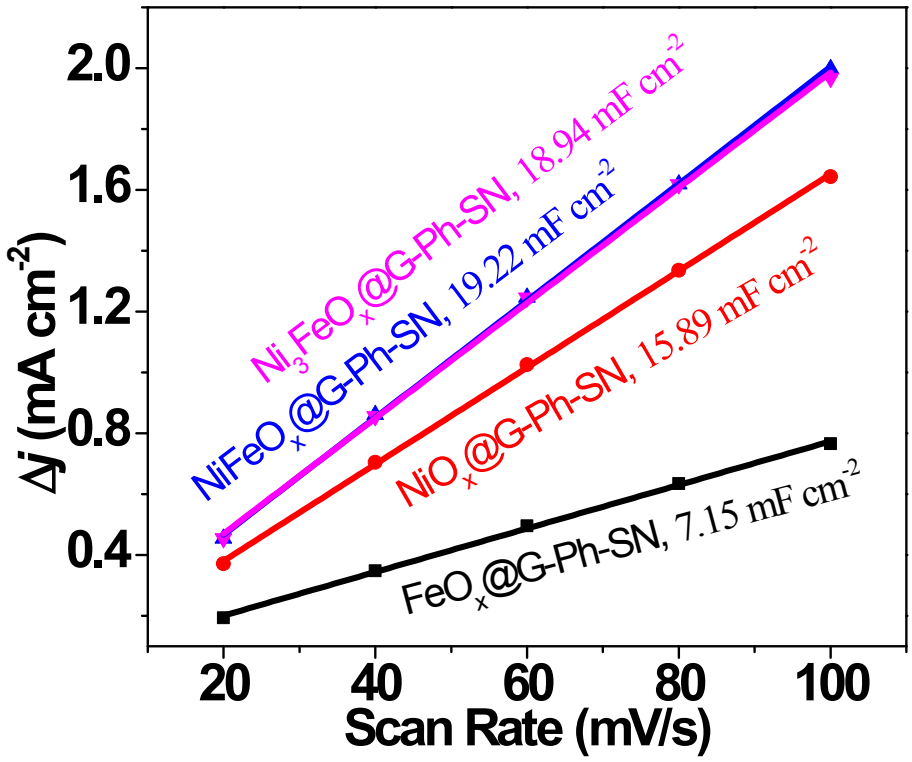

Figure S9. Capacitive *j* vs scan rate for FeO_x@G-Ph-SN, NiO_x@G-Ph-SN, $NiFeO_x$@G-Ph-SN, and Ni_3FeO_x@G-Ph-SN. The linear slope is equivalent to twice of the double-layer capacitance C_{dl}.

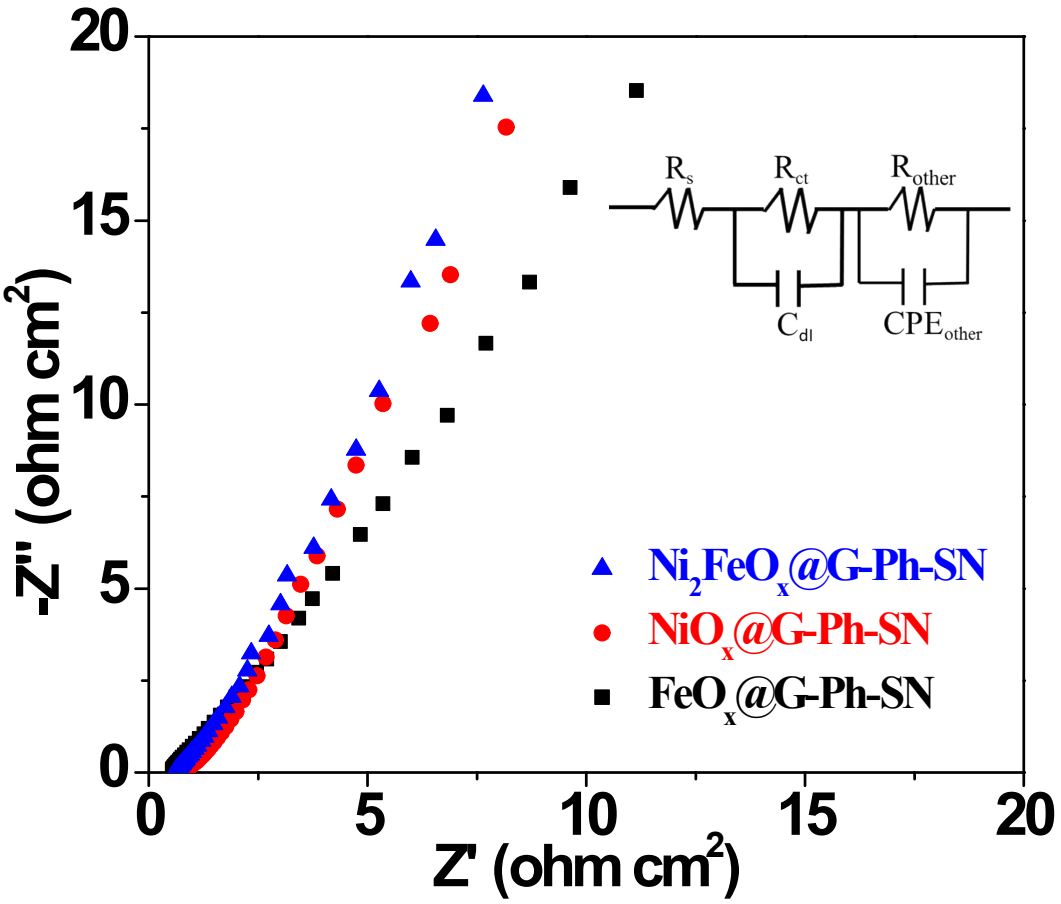

Figure S10. EIS of FeO_x@G-Ph-SN, NiO_x@G-Ph-SN, and Ni_2FeO_x@G-Ph-SN. The inset is an equivalent circuit model.

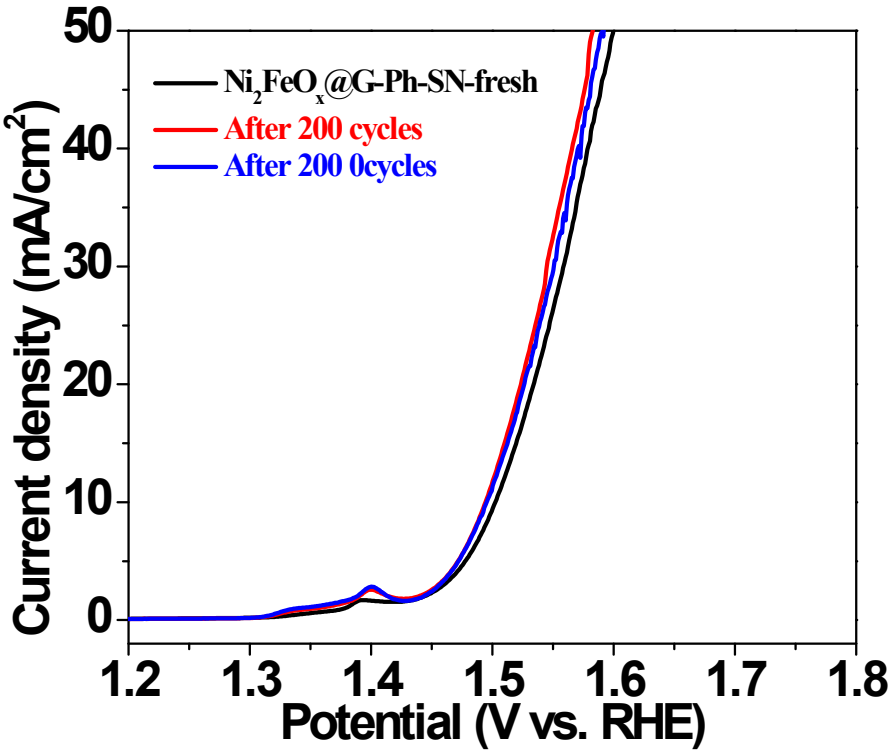

Figure S11. LSV polarization curves of fresh Ni_2FeO_x@G-Ph-SN, Ni_2FeO_x@G-Ph-SN after CV for 200 cycles, and Ni_2FeO_x@G-Ph-SN after CV for 2000 cycles.

Table 1. Comparison of the OER performance of different transition-metal electrocatalysts in 1 M KOH

Catalyst	η@ 10 mA•cm^{-2} (mV)	Tafel slope (mV•dec^{-1})	References
Ni_2FeO_x@G-Ph-SN	265	60.2	This Work
α-$FeCoO_x$	300	33	1
NiFeOOH	340	60	2
NiFe LDH	300	40	3
$Ni_{0.75}Fe_{0.25}OOH$	258	-	4
$NiCo_{2.7}(OH)_x$	350	65	5
CCS Ni-Co	302	43.6	6
Ni-Co LDHs	350	93	7

References

1. M. S. Burke, M. G. Kast, L. Trotochaud, A. M. Smith and S. W. Boettcher, *J. Am. Chem. Soc.*, 2015, **137**, 3638.
2. J. R. Swierk, S. Klaus, L. Trotochaud, A. T. Bell and T. D. Tilley, *J. Phys. Chem. C*, 2015, **119**, 19022.
3. D. Friebel, M. W. Louie, M. Bajdich, K. E. Sanwald, Y. Cai, A. M. Wise, M. J. Cheng, D. Sokaras, T. C. Weng, R. Alonso-Mori, R. C. Davis, J. R. Bargar, J. K. Norskov, A. Nilsson and A. T. Bell, *J. Am. Chem. Soc.*, 2015, **137**, 1305.
4. A. S. Batchellor and S. W. Boettcher, *ACS Catal.*, 2015, **5**, 6680.
5. J. Nai, H. Yin, T. You, L. Zheng, J. Zhang, P. Wang, Z. Jin, Y. Tian, J. Liu, Z. Tang and L. Guo, *Adv. Energy Mater.*, 2015, **5**, 1401880.
6. S.-H. Bae, J.-E. Kim, H. Randriamahazaka, S.-Y. Moon, J.-Y. Park and I.-K. Oh, *Adv. Energy Mater.*, 2017, **7**, 1601492.
7. C. Wang, J. Zhang, C. Shi and D. Cai, *Int. J. Electrochem. Sci.*, 2017, **12**, 10003.